

Pattern computation for compression garment by a physical/geometric approach[☆]

Charlie C.L. Wang^{a,*}, Kai Tang^b

^a Department of Mechanical and Automation Engineering, The Chinese University of Hong Kong, Hong Kong

^b Department of Mechanical Engineering, The Hong Kong University of Science and Technology, Hong Kong

ARTICLE INFO

Article history:

Received 24 June 2008

Accepted 20 February 2009

Keywords:

Physical/geometric modeling
Compression garment

ABSTRACT

This paper addresses the problem of computing planar patterns for compression garments. In the garment industry, the compression garment has been increasingly widely used to retain the shape of a human body, where certain strain (or normal pressure) is designed at some places on the compression garment. Variant values and distribution of strain can only be generated by sewing different two-dimensional (2D) patterns and warping them onto the body. We present a physical/geometric approach for computing 2D meshes that, when folded onto the three-dimensional (3D) body, can generate a user-defined strain distribution through proper distortion. This is opposite to the widely studied mesh parameterization problem, whose objective is to minimize the distortion between the 2D and 3D meshes in angle, area or length.

© 2009 Elsevier Ltd. All rights reserved.

1. Introduction

In the clothing industry, the compression garment has been receiving increasing attention. It is employed plasticize the shape of a human body so that certain specified strain (or compression) can be obtained at some designated places on the body. This type of garment needs to be customized since different bodies have different shapes and thus a different required value and distribution of strain. The 3D body shape can be obtained by any 3D popular data-acquisition means (e.g., a human body laser scanner; see [1,2]). However, it is the 2D patterns – whose corresponding fabricated 3D shape realizes the desired strain distribution – that have to be determined. At present, this 2D pattern design task is accomplished by trial-and-error only, which is inefficient and inaccurate. Moreover, the trial-and-error procedure is costly, as many prototypes have to be produced. Therefore, it is natural to ask for a computer program that can automatically generate 2D patterns from an input 3D shape such that, when fabricated into the final 3D garment, the 2D patterns give the designed strain and pressure on the human body. This motivates the work presented in this paper. Here, we focus only on the task of computing an optimal 2D cloth piece from a given 3D patch, and leave the work of defining cutting curves on 3D human bodies to the

designers. However, in general, pieces with too large area are difficult to satisfy prescribed normal pressures while too small pieces will make the computation have limited degree-of-freedom in optimization.

We exploit a physical/geometric approach to model the relation between the 3D mesh surface and a 2D planar pattern. Every triangle edge on the 3D mesh is considered as a linear truss bar where the force equilibrium equation is established at the tangent plane at each end of the bar. We then establish a formulation that relates the normal pressure at a vertex to all the incident truss bars at the vertex. Geometric constraints are set up at all interior vertices so that the triangles around them can be locally flattened into the plane without distortion when the triangles' edges are given the relaxed length of truss bars. A numerical solution is given in this paper to compute the optimal strain values in the truss bars with the tensile state of the bars ensured (i.e., the garment pieces compress the human body). Fig. 1 gives an example of computing optimal 2D patterns that will generate expected compression configurations.

1.1. Related work

In computer graphics, the pioneer work in [3] provided a general physically-based modeling method for elastic objects, which employs finite-element and finite-difference methods to solve the dynamic governing equations that simulate the deformation of objects like cloth, rubber, metal, etc. Following that work, much effort has been given to improving the simulation of cloth, either in verisimilitude or efficiency aspects, which includes the methods using particle or spring-mass systems [4–11],

[☆] This is an extended version of the paper—*Pattern Computation for Compression Garment*, which is published in ACM Solid and Physical Modeling Symposium 2008, Stony Brook, New York, USA, June 2–4, 2008.

* Corresponding author. Tel.: +852 26098052; fax: +852 26036002.

E-mail address: cwang@mae.cuhk.edu.hk (C.C.L. Wang).

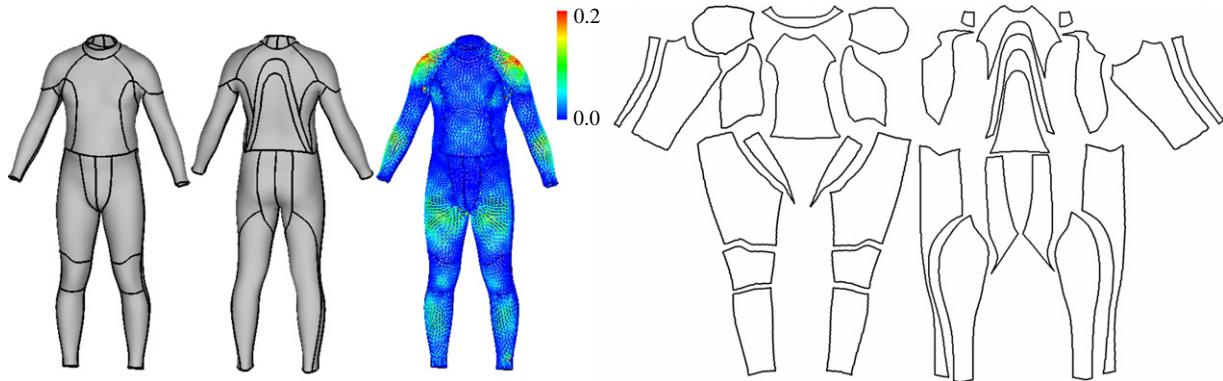


Fig. 1. Computing optimal strain values on 3D garment pieces whose 2D patterns satisfy certain compression requirements. The color map shows the strain distribution on the human body with the suit fabricated from the 2D patterns in the right. (For interpretation of the references to colour in this figure legend, the reader is referred to the web version of this article.)

simulations based on continuum solid mechanics [3,12–16], and numerical schemes that enhance computational stability and speed [8,10,17–19]. Recently, in order to accurately describe the behavior of materials that are strongly resistant to stretch and shear but weakly resistant to bending, the structural buckling model has also been proposed [10,20]. In all of these works, however, the input is a planar pattern (tessellated), and their common purpose is to simulate/predict the 3D shape and motion under some physical theorem. The problem to solve in this paper is the inverse—given a 3D shape and certain associated required physical properties (e.g., strain or pressure), how to determine the 2D patterns that can generate such physical properties. None of the above existing approaches can be directly applied here.

In the literature, another sort of research related to our work is mesh parameterization and surface flattening. Similar to our work here, the parameterization of a given 3D mesh surface is concerned with finding the corresponding 2D parametric domain via surface flattening. In general, a surface parameterization inevitably introduces distortion in either angle or area. All the known parameterization methods are based on how to minimize the distortions (see [21] for a detailed review). Among the abundant literature of mesh parameterization, only a few schemes [22–28] generate a planar domain with a free-boundary so that it can be employed to compute the shape of 2D patterns. However, they never addressed the problem of how to satisfy certain given strain and compression in the 3D shape fabricated from the computed 2D patterns. Different from those approaches are visual results in texture mapping (e.g., [29]) or surface shape in reconstruction (e.g., [30]), where different metrics are derived to optimize a mesh parameterization: the physical laws (e.g., the stress equilibrium) are the major factors to be considered here. In the realm of computer-aided design, the surface flattening for pattern design has been studied from various perspectives (see [31–36]). Nevertheless, neither mesh parameterization nor mesh flattening approaches provides a solution to the physical/geometric problem posed in this paper.

One research area that is perhaps more pertinent to our problem is the study of developable surfaces. From the perspective of differential geometry, developable surfaces inherit many desirable characteristics. There are approaches that either exactly define [37–39] or approximately model [40–42] a 3D shape with developable ruled surfaces. In the latter category, the authors in [43] proposed an approximation scheme that models a given mesh surface with many conical surfaces. Wang and Tang in [44] adopted a discrete Gaussian curvature to process the given mesh surface through constrained optimization, so as to make it as close to being developable as possible. Their work is furthered

in [45] with the introduction of the Flattenable Laplacian (FL) mesh modeling idea, which helps improve the numerical stability. Another related work is the PQ meshes presented in [46], which can also be used to model discrete developable surfaces. All these developable surface modeling methods, exact or approximate, are unfortunately not applicable to our problem, as no distortion is considered in the mapping from a 3D developable surface to its 2D pattern.

Recently, in [47], we proposed a woven-model based geometric approach for the design of elastic medical braces, where the elastic brace worn by a human body is simulated by a woven model with orthogonal warp and weft threads. In that work, the elastic behavior is simulated by three types of spring: warp, weft and diagonal. An elastic energy is formulated with these springs, and a diffusion process is adopted to minimize the elastic energy that determines the distribution of woven nodes on the given 3D surface, so as to obtain the desired 3D-to-2D mapping. There are, however, serious deficiencies in the approach of [47]; specifically as follows:

- Only the elasticity in two directions – warp and weft – is considered; therefore, when in equilibrium, the strain (and stress) on a single weft or warp thread is a constant. The result is that only very simple patterns of strain distribution can be simulated by the woven model.
- The computation of re-distributing the woven nodes on the surface is based on the knowledge of a strain distribution. However, computing such strain distribution in general is not straightforward. And thus, again, the woven-model based approach in [47] can only mimic very simple and limited patterns of strain distribution.
- The strains on the springs around a point with a user-specified normal pressure is calculated by fitting a quadratic polynomial. Such an approximation is not accurate enough.
- The boundary of the woven model takes a zigzag-like shape, which causes great difficulty in modeling the physical interactions between the 2D pieces that will have to be sewed together.
- There is no guarantee that all the threads will be in the tensile state, which is strongly required by a compression garment.

1.2. Contribution

To overcome the above deficiencies, we develop a new physical/geometric approach in this paper that is able to model more complicated elastic behaviors of fabrics, and determine the 2D patterns of a given 3D mesh surface satisfying the given strain and/or normal pressure distribution. In this new model, every triangle edge is simulated by a tensile truss bar,

and the equilibrium equation is established at every vertex on the given mesh surface. The relationship between the normal pressure and the stress on the truss bars is also carefully analyzed. Moreover, critical geometric constraints are introduced to ensure that the network of trusses in the relaxed state can be flattened without significant stretch. The sewing behavior between assembled patches is also modeled. After all these modules have been assembled together, the strain distribution on the truss bars is finally determined with a least-square based iterative minimization.

The rest of the paper is organized as follows. Section 2 describes the physical models for the compression garment. The geometric constraints for the distortion-free flattening are given in Section 3. In Section 4, the physical model and the geometric constraints are integrated and a linearization is proposed for the resulting system (which is highly nonlinear) so that it can be iteratively solved with least-square solutions. Some test results are provided in Section 5, followed by the conclusion and discussion section.

2. Physical model

Without loss of generality, the input 3D surface M is assumed to be represented by a triangular mesh. To simulate the physical behavior of elastic fabrics on M , every triangle edge is considered to be a linear truss bar. The human body that supports the elastic fabrics is defined by a given 3D shape H . The following definitions and assumptions are imposed on the physical model of our compression garment.

Definition 1. The given triangular mesh surface M is a piece of elastic fabric in its final shape when it is worn on H .

Definition 2. The elastic fabric is represented as a network of linear truss bars in connectivity on M .

Assumption 1. All the linear truss bars are of a same material, and of the same cross section.

From the study of elastic materials [48], the strain of a linear truss bar e is

$$\varepsilon_e = (l_e - l_e^0)/l_e^0 \quad (1)$$

where l_e is the current length of e and l_e^0 is length in the relaxed state. The relation between the strain ε_e and the stress σ_e of e is

$$\sigma_e = k\varepsilon_e. \quad (2)$$

The force according to this stress is its integral over the entire cross section of the truss bar. By Assumption 1, the stiffness coefficient k in Eq. (2) is constant over the entire fabric, and the relationship between the strain and the force is linear. This simplifies the later formulation in the paper, for otherwise the equilibrium equation introduced below would become nonlinear and make the problem much more difficult to solve.

Definition 3. For a compression garment, the strain ε_e on every truss bar e should satisfy $\varepsilon_e \geq 0$.

Definition 4. For a linear truss bar e , its generated force f_e is proportional to its strain ε_e with a constant ratio.

Assumption 2. The nodes linking the truss bars are coincident with the vertices of M when the whole truss structure is in equilibrium.

Assumption 3. The friction between the elastic fabric and the surface of human body is negligible.

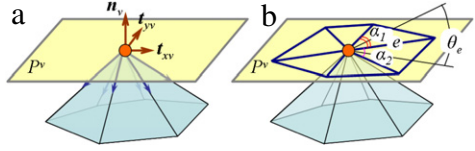


Fig. 2. Illustration for the physical model at an interior vertex.

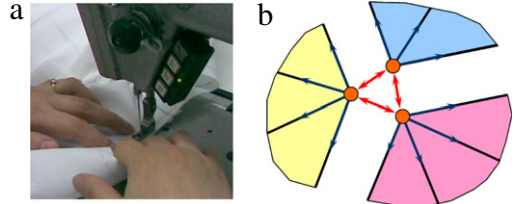


Fig. 3. Illustration for the sewing model—the blue arrows are forces generated by the tensile truss bars to the nodes, and the red ones are the reaction forces between sewing nodes. (For interpretation of the references to colour in this figure legend, the reader is referred to the web version of this article.)

Assumption 4. The human body H under compression agrees with the shape of M , and the deformation of H is neglected.

The forces at every joint node of the truss structure should be in equilibrium so that the whole system is in a stable state. Based on this assumption, we can derive the following lemma.

Lemma 1. *The projection of forces in the tangent plane, P^v , to a node $v \in M$ as generated by the truss bars around v , is in equilibrium.*

Proof. Let f_e be the force on truss bar $e \in E(v)$ with $E(v)$ denoting the collection of edges linking to v . f_e can be decomposed into the component perpendicular to P^v and that in P^v . By Assumptions 2 and 3, the perpendicular component is balanced by the support from the human body and the friction is ignored. Therefore, we have the following equilibrium equation in the plane P^v :

$$\sum_{e \in E(v)} P^v(f_e) \equiv 0 \quad (3)$$

where $P^v(\cdot \cdot \cdot)$ stands for the projection of a vector onto the plane P^v . Fig. 2(a) gives an illustration for this. \square

Motivated by the strain–stress theories in solid mechanics [49], we stipulate that the relationship between the tensile strain and the normal curvature can be modeled as

$$p_v = s \int_0^{2\pi} \kappa_n(\theta) \sigma(\theta) d\theta \quad (4)$$

where $\kappa_n(\theta)$ is the normal curvature in direction θ on the tangent plane at the surface point, $\sigma(\theta)$ denotes the normal stress in θ , and s is a parameter to reflect the effect on different materials. Here, we reasonably further simplify the formula into a finite sum on the truss structure model as

$$p_v = \frac{s}{2\pi\kappa_H} \sum_{e \in E(v)} (-t_e \cdot n_v) \theta_e \varepsilon_e \quad (5)$$

where t_e is the unit vector of truss bar e pointing outwards from v , n_v is the unit normal vector to surface M at v , κ_H is the mean curvature at v , and θ_e reflects the weights of the truss bar e contributing to the normal pressure. Here, the value of θ_e is the average angle of e 's left and right triangles at the vertex v on P^v . As illustrated in Fig. 2(b), $\theta_e = 0.5(\alpha_1 + \alpha_2)$.

In practice, the 2D patterns of a compression garment are sewed together by suture (see Fig. 3(a)). We need to model the physical

effect of this sewing operation. Generally speaking, during sewing, the boundaries of fabrics are in the relaxed state. If some distortion is introduced after the pieces are sewed together, unwanted wrinkles might occur and thus violate the original design intent—this is one critical criterion to evaluate whether a garment is well designed and fabricated. Since the suture in general is not elastic, the boundaries of fabrics locked by suture have almost no freedom of deformation. Therefore, we introduce the following definition and assumption in our physical model.

Definition 5. The boundary of a given mesh surface M is defined as a *sewn-boundary* if it is linked to other pieces by suture; otherwise, it is defined as a *free-boundary*.

Assumption 5. For the truss bars overlapping the boundary of a fabric piece, their strain should be zero when the system of truss structure is in equilibrium.

Note that the above assumption is only for a sewn-boundary; the strain may not be zero for free-boundaries (e.g., the free-boundary of elastic braces shown in Fig. 6(c)). Moreover, for the input mesh surfaces to be assembled together, we assume that they are stitched together by making the boundary vertices coincident (e.g., as shown in Fig. 3(b), three pieces – in different colors – are stitched together by linking the three orange vertices). The reaction forces among them would resist this stitching. Therefore, the equilibrium at the sewing nodes relies on the forces from truss bars linked to all these nodes. More specifically, Eq. (3) given above needs to be modified as

$$\sum_{e \in E(v)} P^v(f_e) + \sum_{v_s \in S(v)} \sum_{e \in E(v_s)} P^v(f_e) \equiv 0 \quad (6)$$

where $S(v)$ denotes the collection of all nodes that should be sewed together with node v during the fabrication.

The physical model developed in this section will work together with the geometric constraint derived next to satisfy the physical properties of compression garment on the 3D shape warped from the computed 2D patterns.

3. Geometric constraint

The behavior of elastic fabric pieces on a compression garment should not only be governed by the equilibrium equation (i.e., Eqs. (3) and (6)) described in the previous section, but also have correct geometric constraints to ensure that the 3D shape can really be fabricated from 2D patterns. This leads to the following developability constraints imposed on every interior mesh vertex.

From differential geometry, it is well known that a surface can be developed into two dimensions without local stretch only if the Gaussian curvature is zero everywhere on it. When dealing with a piecewise linear mesh surface, the Gaussian curvature is converted to the form in terms of the angles of triangles at the involved vertex, which has been successfully used in several existing systems (e.g., [22,27,44,45]). Therefore, we use a similar formula to constrain the local geometry of a fabric piece for compression garment.

For a vertex v on M , using $\alpha_f(v)$ to symbolize the vertex angle of triangular face f at v , the condition

$$\sum_{f \in F(v)} \alpha_f(v) \equiv 2\pi$$

should be satisfied if all the faces f around v are to be flattened without any cracks and/or overlapping, where $F(v)$ is the set of triangles incident at v . Note that, in our problem setting, the triangles in three dimensions have already been purposely distorted in order to generate compression. Therefore, we must use the angle of face f in its original relaxed state to replace $\alpha_f(v)$.

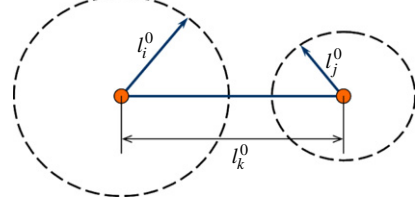


Fig. 4. Invalid edges that fail the triangle construction.

Constraint 1. Let $\alpha_f^0(v)$ represent the angle of the relaxed triangle f at v ; the geometric constraint at an interior vertex v is defined as

$$\sum_{f \in F(v)} \alpha_f^0(v) \equiv 2\pi. \quad (7)$$

Note that this constraint is only set for interior vertices. For boundary vertices, the constraint in terms of angles should be

$$\sum_{f \in F(v)} \alpha_f^0(v) < 2\pi. \quad (8)$$

During the computation of planar patterns, we seek to determine the optimal original length of each truss bar so that the above geometric constraint and the equilibrium equations can be satisfied (in the minimum energy sense). The *triangle constraint* defined below is also important and necessary, as it ensures the validity of the lengths of a truss bar.

Constraint 2. Let l_1^0, l_2^0 and l_3^0 represent the relaxed lengths of three bars e_1, e_2 and e_3 in a triangle in M ; they must satisfy

$$l_i^0 + l_j^0 - l_k^0 > 0 \quad (9)$$

if $l_k^0 \geq l_i^0$ and $l_k^0 \geq l_j^0$ with $ijk \in \text{permutation of } \{1, 2, 3\}$.

The inequality constraint in Eq. (9) prevents the scenario shown in Fig. 4 from happening.

4. Numerical solution

This section presents the numerical scheme that computes the optimal tensile strain on every linear truss bar so that the given normal pressure distribution on M can be realized (in the minimum energy sense). Nodes are not moved during the computation in our approach. The user is allowed to specify the desired normal pressure at some designated vertices on M (referred to as anchor points). Note that this does not mean that the normal pressures are only on isolated vertices. We choose to define pressure in this way is only because it is an easy method for users to specify their requirements. As a direct result of the tensile strains on M , the corresponding 2D patterns of M are also obtained. The optimal strains should ensure the force equilibrium at all the vertices (i.e., joint nodes of the truss structure), realize the given normal pressures, and also satisfy the geometric constraints Eqs. (7)–(9).

The intuitive variables in the numerical system are the strain ε_e on truss bars. Instead, to safeguard the $\varepsilon_e \geq 0$ requirement (as in Definition 3), we introduce a new variable x_e as

$$\varepsilon_e = x_e^2. \quad (10)$$

Per Lemma 1, the projection of forces of truss bars around a vertex v onto its tangent plane should be in equilibrium. According to Assumption 1, the forces are proportional to the strains on truss bars. Therefore, the equilibrium equation (i.e., Eq. (3)) can be derived to become

$$\begin{aligned} \sum_{e \in E(v)} (t_{xv} \cdot t_e) f_e &= \sum_{e \in E(v)} (t_{xv} \cdot t_e) \sigma_e = \sum_{e \in E(v)} (t_{xv} \cdot t_e) k \varepsilon_e = 0 \\ \sum_{e \in E(v)} (t_{yv} \cdot t_e) f_e &= \sum_{e \in E(v)} (t_{yv} \cdot t_e) \sigma_e = \sum_{e \in E(v)} (t_{yv} \cdot t_e) k \varepsilon_e = 0 \end{aligned}$$

with f_e and σ_e the tensile force and stress on the truss bar e , and then

$$\sum_{e \in E(v)} (t_{xv} \cdot t_e) x_e^2 = 0, \quad \sum_{e \in E(v)} (t_{yv} \cdot t_e) x_e^2 = 0 \quad (11)$$

where t_{xv} and t_{yv} are the unit vectors of the local frame established at v such that $n_v = t_{xv} \times t_{yv}$ (i.e., n_v , t_{xv} and t_{yv} are orthogonal to each other as illustrated in Fig. 2(a)). Similar formulas can be derived from Eq. (6) for nodes that are sewn together on the boundaries. These equations should be satisfied on all vertices of M . Also, by Assumption 5, we should let $x_e = 0$ for those truss bars on the sewn-boundary.

Γ represents the collection of all the anchor vertices with some prescribed normal pressure. The strain-pressure conversion equation derived from Eq. (5) is defined on every vertex $v \in \Gamma$ by replacing ε_e in Eq. (5) with x_e^2 .

The equations for geometric constraints are also reformulated in terms of x_e , and the relaxed length l_e^0 is converted into $l_e^0 = l_e / (1 + x_e^2)$ with the length of truss bar e , l_e , on the given mesh surface M . The inequality constraints are introduced into the numerical system by the active set method. In short, the inequality constraints are partitioned into an active set and an inactive set—only the constraints in the active set are added into the system during computation (see [50]).

4.1. Linearization and least-square solution

Almost all the above-listed equations are nonlinear in nature. To device a numerical solution for them, we first linearize the equations and then utilize the least-square method to iteratively update the value of x_e , till a satisfactory solution is obtained.

The linearization is obtained by the first-order Taylor expansion. Explicitly, Eq. (11) is linearized to

$$\sum_{e \in E(v)} (t_{xv} \cdot t_e) x_e^2 + \sum_{e \in E(v)} 2(t_{xv} \cdot t_e) x_e \delta_e \approx 0 \quad (12)$$

$$\sum_{e \in E(v)} (t_{yv} \cdot t_e) x_e^2 + \sum_{e \in E(v)} 2(t_{yv} \cdot t_e) x_e \delta_e \approx 0 \quad (13)$$

where $\delta_e = x_e^{new} - x_e$ and x_e is the current value for the truss bar e . The formulas have an approximation error $O(\delta_e^2)$. For the normal pressures assigned on the anchor points, Eq. (5) can be converted into a linear form in terms of δ_e as

$$p_v \approx s \sum_{e \in E(v)} a_e x_e^2 + 2s \sum_{e \in E(v)} a_e x_e \delta_e \quad (14)$$

where $a_e = (-t_e \cdot n_v) \theta_e / 2\pi \kappa_H$ and the approximation error is $O(\delta_e^2)$.

As for the geometric constraint (Eq. (7)), the value of $\alpha_f^0(v)$ depends not only on the strain of bars incident at v but also on the bars opposite to v (see Fig. 5). Therefore, applying the Taylor expansion to Eq. (7) leads to

$$\alpha_v + \sum \frac{\partial \alpha_v}{\partial l_e^0} \frac{\partial l_e^0}{\partial x_e} \delta_e + \sum \frac{\partial \alpha_v}{\partial l_{opp}^0} \frac{\partial l_{opp}^0}{\partial x_{opp}} \delta_{opp} \approx 0 \quad (15)$$

where $\alpha_v = \sum_{f \in F(v)} \alpha_f^0(v)$ is the current vertex angle at v , l_e^0 is the relaxed length of the truss bars adjacent to v , and l_{opp}^0 is the relaxed length of bars opposite to v . Regarding the derivatives (see Fig. 5), we have $\partial \alpha_v / \partial l_e^0 = \partial(\alpha_1 + \alpha_2 + const) / \partial l_e^0$, where α_1 and α_2 are in terms of $(l_e^0, l_{next}^0, l_{opp1}^0)$ and $(l_e^0, l_{last}^0, l_{opp2}^0)$, respectively, and $\partial \alpha_v / \partial l_{opp}^0 = \partial \alpha / \partial l_{opp}^0$, with α depending on $(l_1^0, l_2^0, l_{opp}^0)$ by the $\arccos(\dots)$ function. Note that all the angles here are evaluated by the relaxed lengths of truss bars (i.e., l_e^0) instead of their current lengths. A similar linearization can be applied to Eq. (8) for the

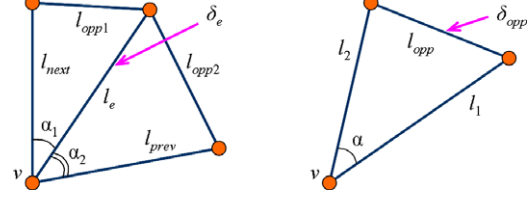


Fig. 5. The derivative of vertex angle in terms of the strain. Left, the variable δ_e is for the bar adjacent to the vertex v ; right, the variable δ_{opp} is for the bar opposite to the vertex.

boundary vertices, which leads to the same formula as Eq. (14)—note that this linear equation about boundary vertices is added into the numerical system only when Eq. (8) is not satisfied.

For the triangle constraint, when Eq. (9) is disobeyed, the following linearization of it is inserted into the numerical system.

$$l_i^0 + l_j^0 - l_k^0 + \frac{\partial l_i^0}{\partial x_i} \delta_i + \frac{\partial l_j^0}{\partial x_j} \delta_j - \frac{\partial l_k^0}{\partial x_k} \delta_k \approx 0. \quad (16)$$

To cater for the sewing constraint (Eq. (6)), we first linearize Eq. (6) in a way exactly similar to that of Eqs. (12) and (13). Then, owing to Assumption 5, we let

$$\delta_e + x_e = 0 \quad (17)$$

for any truss bar e on a sewn-boundary.

Furthermore, in order to add damping factors to make the numerical system more stable, we wish that the update of x_e for all non-sewn-boundary bars is small in each iteration step. Therefore, we introduce the following damping equation into the numerical system for all truss bars except the ones on a sewn-boundary:

$$\delta_e = 0. \quad (18)$$

Note that as the least-square solution will be used to determine the value of δ_e , the value of δ_e at interior bars will be a balanced value from all constraints in Eqs. (12)–(18) but not zero.

Integrating all the above linear equations (Eqs. (12)–(18)) together, we have

$$\begin{bmatrix} A \\ I \end{bmatrix} [\delta_e] = \begin{bmatrix} b_a \\ b_i \end{bmatrix} \quad (19)$$

where A and b_a are derived from Eqs. (12)–(16), and b_i is from Eqs. (17) and (18). This is an over-determined linear equation system, which can be solved by the least-square solution as

$$\begin{bmatrix} A^T & I \end{bmatrix} \begin{bmatrix} A \\ I \end{bmatrix} [\delta_e] = \begin{bmatrix} A^T & I \end{bmatrix} \begin{bmatrix} b_a \\ b_i \end{bmatrix}. \quad (20)$$

In our implementation, after giving initial values for $x = [x_e]$, iteratively, we solve Eq. (20) and then update the values of x by $x \leftarrow x + \delta$. The iteration continues until either the zero-norm condition $\|\delta\|^2 < 10^{-5}$ is met or the maximum number of iterations (e.g., 500) is reached. To different rows in the linear system of Eq. (19), different weights may be adopted. In all our tests, we multiply both sides of the equations from Eq. (15) with a weight of 5.0 (as compared to a weight of 1.0 for all the other rows), so as to highlight the developability constraint. Regarding the weights on anchor points, we assign a weight $N_v(M)/N_v(\Gamma)$, with $N_v(M)$ the number of vertices on M and $N_v(\Gamma)$ the number of anchor points.

4.2. Computing the 2D shape

After the optimal values of x_e are determined, the relaxed lengths of all the truss bars can be calculated. The only task left

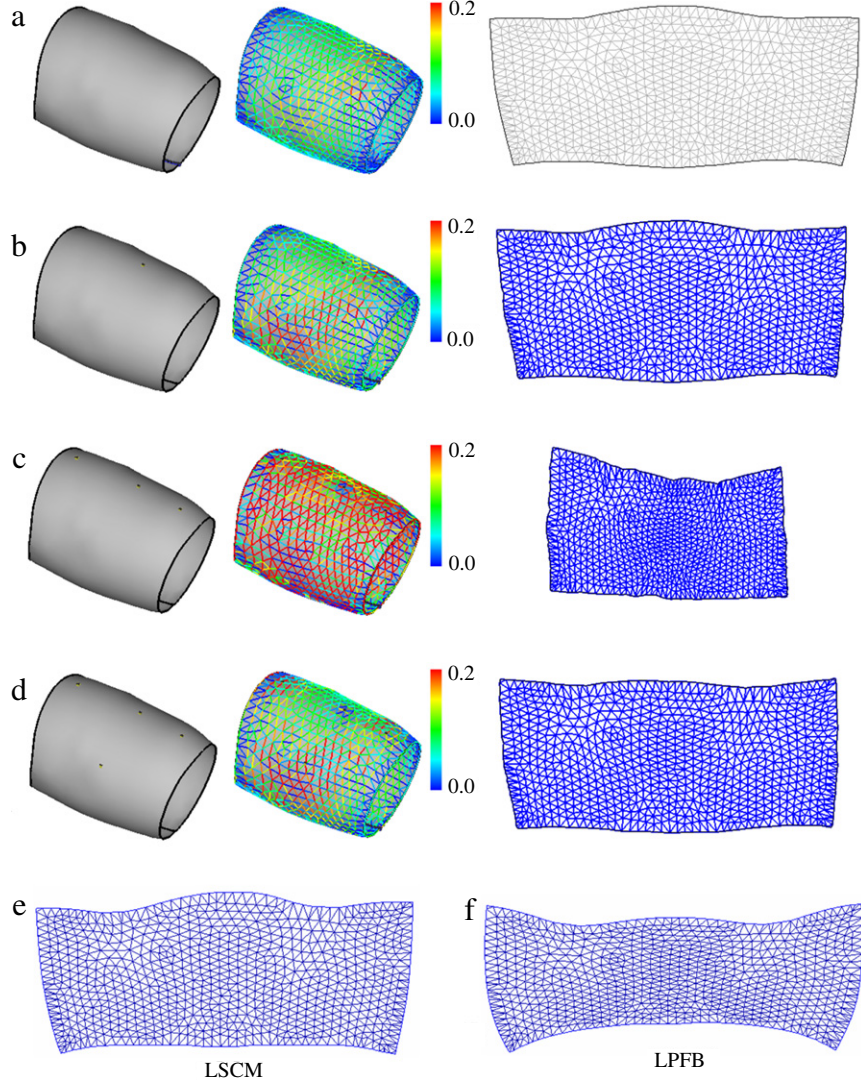


Fig. 6. The medical brace example with different normal pressures specified at the anchor points (colored black): (a) the brace is free—no specific normal pressure is assigned, (b) brace A—with one anchor point, (c) brace B—with three anchor points, and (d) brace C—with four anchor points. The color maps show different strain distributions corresponding to the four different normal pressure configurations. The final 2D patterns are also given (in red): they are superimposed with the one from the free brace in (a), for comparison. (e) and (f) give the planar meshes generated by the least-squares conformal map (LSCM) and the length-preserved free-boundary (LPFB) respectively, which are very different from the patterns generated by this approach. (For interpretation of the references to colour in this figure legend, the reader is referred to the web version of this article.)

is to determine the 2D shape of each pattern. For that, we first compute the angles in all triangles by the relaxed lengths of triangle edges. Then, the angle-based least-square formulation [27] is used to determine the 2D coordinates of each vertex. By the method proposed in [27], we fix the position of two vertices on the longest edge and solve a set of linear equations relating angles to the planar coordinates. The reason why we did not adopt the intuitive greedy reconstruction is that, while the flattening of each triangle alone generates a very small numerical error, these errors accumulate at the front. Thus, when the involved mesh surface has many triangles, the accumulated error at the end could be very large. The least-square reconstruction somewhat balances out the cumulative error. The 2D mesh obtained can be further optimized by the method in [35].

5. Experimental results

We have implemented the proposed method in a prototype program written in C++. Several experimental results are given in this section. Before that, we first define some error measurement terms for the evaluation of the test results.

The first error item is the deviation between the pre-specified desired normal pressure and the computed normal pressure on M , as

$$E_p = \frac{1}{m_a} \sum_v |p_v - p_v^0| \quad (21)$$

where m_a is the number of anchor points, p_v^0 is the desired normal pressure, and p_v as the one defined by Eq. (5). In our tests, the s in Eq. (5) is simply assigned with the value 1.0, although some more realistic values could be calibrated, depending on the physical knowledge of the model, such as the material of the garment, etc.

The second error item measures the level of equilibrium at the vertices in the final M , as

$$E_F = \sum_e \|(\mathbf{t}_e \cdot \mathbf{t}_x) \varepsilon_e\|^2 + \sum_e \|(\mathbf{t}_e \cdot \mathbf{t}_y) \varepsilon_e\|^2. \quad (22)$$

While these two error items relate to the physical property of the system, the following two

$$E_{\theta\text{mean}} = \frac{1}{m_{\text{int}}} \sum_v \left| 2\pi - \sum_{f \in F(v)} \alpha_f^0(v) \right| \quad (23)$$

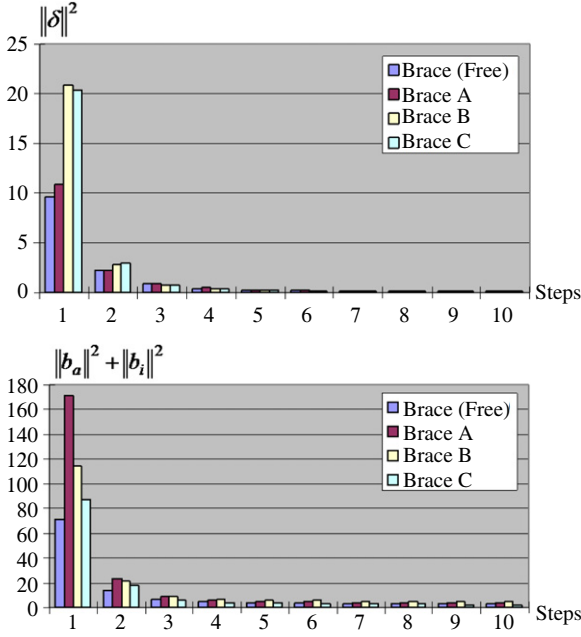


Fig. 7. Convergence of the numerical iterations for the example of Fig. 6, in terms of $\|\delta\|^2$ (top) and $\|b_a\|^2 + \|b_i\|^2$ (bottom).

$$E_{\theta_{\max}} = \max \left\{ \left| 2\pi - \sum_{f \in F(v)} \alpha_f^0(v) \right| \right\} \quad (24)$$

quantify the developability of the final M, i.e., how well it can be flattened. m_{int} is the number of non-boundary vertices on M. Note that $\alpha_f^0(v)$ is computed with the relaxed lengths of the truss bars in the triangle f . The final error item, E_L , is used to measure the length change on the flattened patterns from the original relaxed value l_e^0 , as

$$E_L = \frac{1}{m_e} \sum_e |l_e^0 - l_e^*|/l_e^0 \quad (25)$$

where l_e^* is the length of edge e after being flattened and m_e is the number of truss bars (i.e., edges) on M.

We tested the developed model on a medical elastic brace example with four different configurations of normal pressure assignment. In Fig. 6, (a)–(d) display the results of strain distribution and planar patterns under different normal pressure assignments. It is worth mentioning that the configuration in Fig. 6(d) can never be simulated by the method in [47]. For comparison, the 2D patterns generated by the least-squares conformal map (LSCM) [25] and the length-preserved free-boundary (LPFB) [51] are given in Fig. 6(e) and (f). Table 1 lists the error measurements on the results of the four configurations, all of which are small, indicating that the numerical iterations converged for all the four configurations in the test. To investigate the speed of convergence, we recorded the value of $\|\delta\|^2$ and $\|b_a\|^2 + \|b_i\|^2$ after each iteration step for these four configurations, which are shown in Fig. 7. It is seen clearly from the figure that both norms drop quickly after few iterations. On the other hand, the convergence speed became noticeably slower after certain threshold values of the norms—in our tests, the value of $\|\delta\|^2$ never became smaller than 10^{-5} , even after some large number of iterations (e.g., 500). This is similar to other iterative numerical schemes.

We have successfully applied the proposed method to a wetsuit design project currently underway in our laboratory (see Fig. 1), in which the objective is to determine the 2D patterns of neoprene pieces that are used to fabricate the wetsuit. Fig. 8 shows the results of both free (without normal pressure assignment) and constrained (with normal pressure assignment) cases.

Table 1
Statistics of errors.

Example	E_P	E_F	$E_{\theta_{\text{mean}}}$	$E_{\theta_{\text{max}}}$	E_L
Brace (free)	N/A	2.7×10^{-4}	3.4×10^{-4}	0.036	5.7×10^{-3}
Brace A	6.0×10^{-6}	1.6×10^{-3}	7.4×10^{-4}	0.038	1.7×10^{-2}
Brace B	1.6×10^{-4}	3.2×10^{-3}	2.8×10^{-3}	0.037	1.5×10^{-2}
Brace C	7.0×10^{-5}	4.2×10^{-4}	7.8×10^{-4}	0.038	2.4×10^{-2}

Table 2
FEA tests on neoprene cylinders.

Radius R (mm)	Pressure (N/m ²)	Strain
64.75	150	0.9675
64.75	100	0.6450
64.75	50	0.3225
54.75	150	0.8176
54.75	100	0.5450
54.75	50	0.2725

The neoprene has Young's Modulus 1.85 GPa and density 1210 kg/m³.

5.1. Verification by finite element analysis

In order to verify the proposed physical/geometric approach, we compare the results computed by our scheme with the simulation results from finite element analysis (FEA). Two cylinder models under different compressions are tested by the commercial FEA software Algor [52]. As shown in Fig. 9, the uniform normal pressures are added onto the cylinder, and the strain distribution can be generated by the system. We measure the strain at the red point shown in the right figure and obtain the results listed in Table 2. It is not difficult to find that the value of strain is approximately proportional to the normal pressure loadings and the radius of the cylinder (i.e., inverted to the curvature).

We test the two models by our approach with the specified normal pressure 50 N/m². By Eq. (5), we know that if the values of the normal pressure p_v and the strain ε_e on all truss bars are known, the value of s can be determined. In this test, we use the results from FEA to give a virtual calibration to obtain the value $s = 242.56$. The computed 2D patterns have an average length of 269.32 mm (for the cylinder with $R = 54.75$ mm) and 305.33 mm (for the cylinder with $R = 64.75$ mm), and thus will give a strain (i.e., stretch) of

$$\varepsilon = (2\pi \times 54.75 - 269.32)/269.32 \simeq 0.277$$

and

$$\varepsilon = (2\pi \times 64.75 - 305.33)/305.33 \simeq 0.332$$

on the warped 3D patches as shown in Fig. 10. These values of strain are very close to the results from FEA.

6. Summary and discussion

The main goal of this paper is to propose a numerical algorithm that, given a 3D mesh surface M and certain prescribed tensile strain values at some designated points on M, computes a suitable flattened 2D pattern of M that, when folded back to M, will best realize the prescribed strain. By means of the elementary strain-stress relationship from solid mechanics, the proposed method can be directly used for the design of a compression garment (e.g., the wetsuit and the elastic medical assistant braces), where the prescription of normal pressure, instead of strain, is usually desired. The proposed method comprises a carefully established system of equilibrium and geometric constraints – that maintains the integrity of the underlying physical/geometric properties – and a numerical solution, based on linearization and least-squares solution, for solving the system.

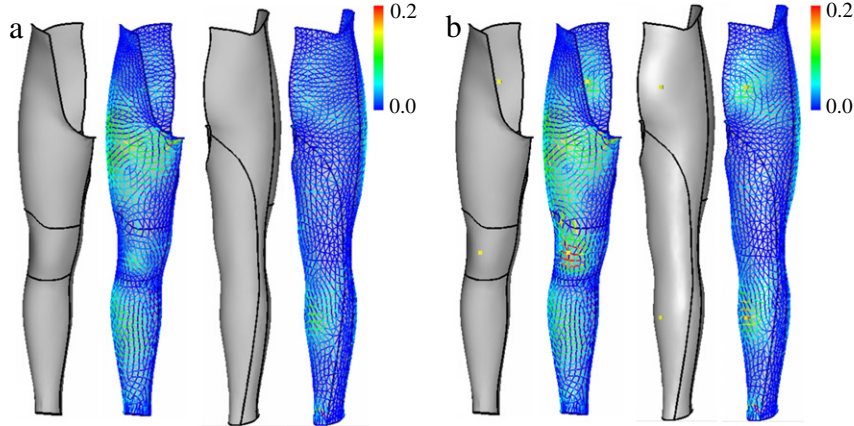


Fig. 8. The lower body of a wetsuit example—(a) without normal pressure assignment, and (b) with normal pressures specified at anchor points (colored yellow). (For interpretation of the references to colour in this figure legend, the reader is referred to the web version of this article.)

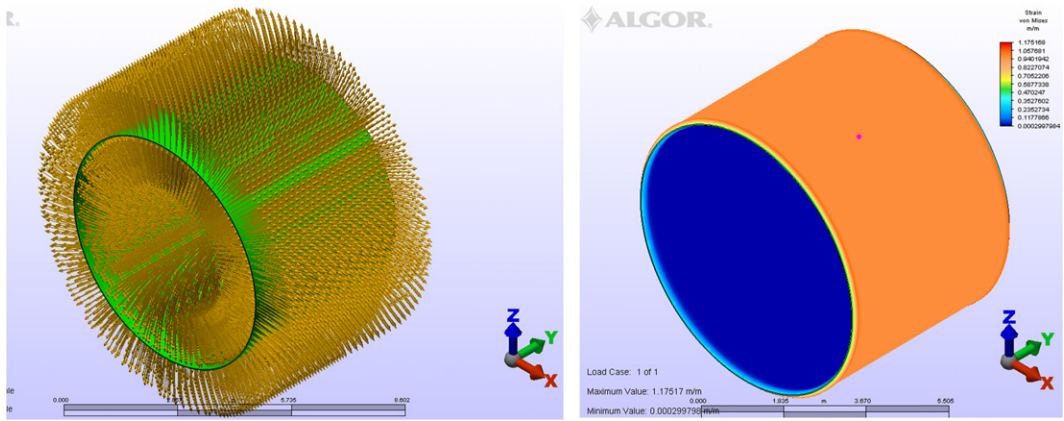


Fig. 9. Testing the pressure–strain relationship by FEA software.

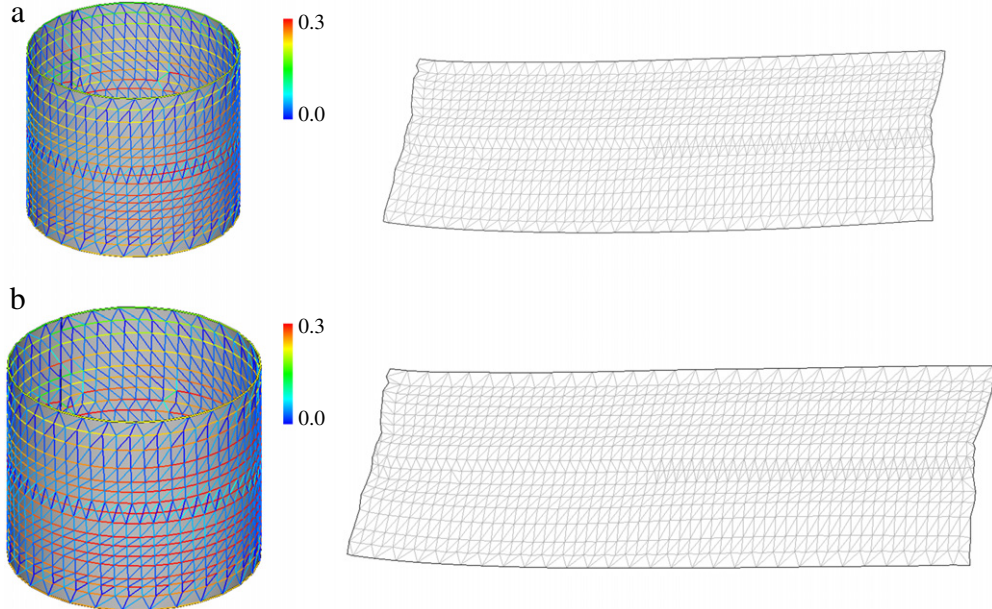


Fig. 10. The results by our approach on cylinders with different radius with normal pressure 50 N/m^3 at an anchor point: (a) the average length of the resultant pattern is 269.32 mm ($R = 54.75 \text{ mm}$), and (b) the average length of the resultant pattern is 305.33 mm ($R = 64.75 \text{ mm}$).

Similar to other computational engineering applications using triangular meshes (e.g., finite element analysis), the accuracy of computation here will be greatly affected by the quality of the

meshes. An ideal mesh should have every facet near a regular triangle. A remeshing step [53] is usually employed to pre-process the mesh surface before applying our approach in this paper.

Our initial computer simulation tests of the proposed algorithm have shown some promising results. However, in order for it to be an effective tool for real industrial applications, such as the design of medical braces, more work – especially physical calibration and experiments to determine the material-oriented coefficient, s , in our approach – is needed, and this will be our subsequent work.

Acknowledgements

This work is partially supported by Hong Kong Innovation and Technology Fund (ITS/026/07), CUHK Direct Research Grant (CUHK/2050374 and CUHK/2050400), and Shun Hing Institute of Advanced Engineering (SHIAE) Research Grant (CUHK/8115022). The authors would like to thank Mr. Long Ho Chau for help in generating the FEA simulation results.

References

- [1] Cyberware. 2005. <http://www.cyberware.com>.
- [2] TC2. 2005. <http://www.tc2.com>.
- [3] Terzopoulos D, Platt J, Barr A, Fleischer K. Elastically deformable models. In: Proceedings of ACM SIGGRAPH. vol. 87. 1987. p. 205–14.
- [4] Carignan M, Yang Y, Magnenat-Thalmann N, Thalmann D. Dressing animated synthetic actors with complex deformable clothes. In: Proceedings of ACM SIGGRAPH. vol. 92. 1992. p. 99–104.
- [5] Volino P, Courchesne M, Magnenat-Thalmann N. Versatile and efficient techniques for simulating cloth and other deformable objects. In: Proceedings of ACM SIGGRAPH. vol. 95. 1995. p. 137–44.
- [6] Provot X. Deformation constraints in a mass-spring model to describe rigid cloth behavior. In: Proceedings of graphics interface. 1995. p. 147–54.
- [7] Volino P, Magnenat-Thalmann N, Shen J, Thalmann D. An evolving system for simulating clothes on virtual actors. IEEE Computer Graphics and Applications 1996;16(5):42–51.
- [8] Baraff D, Witkin A. Large steps in cloth simulation. In: Proceedings of ACM SIGGRAPH. vol. 98. 1998. p. 43–54.
- [9] Desbrun M, Schröder P, Barr A. Interactive animation of structured deformable objects. In: Proceedings of graphics interface. 1999. p. 1–8.
- [10] Choi K-J, Ko H-S. Stable but responsive cloth. ACM Transactions on Graphics 2002;21(3):604–11.
- [11] Bridson R, Marino S, Fedkiw R. Simulation of clothing with folds and wrinkles. In: Proceedings of ACM SIGGRAPH/Eurographics symposium on computer animation. 2003. p. 28–36.
- [12] Ascough J, Bez H, Bricis A. A simple beam element, large displacement model for the finite element simulation of cloth drape. Journal of the Textile Institute 1996;87(1):152–65.
- [13] Tan S, Wong T, Zhao Y, Chen W. A constrained finite element method for modeling cloth deformation. The Visual Computer 1999;15(2):90–9.
- [14] Eischen J, Biglani R. Continuum versus particle representations. In: House D, Breen D, editors. Cloth modeling and animation. A.K. Peters, Ltd.; 2000. p. 79–122.
- [15] Grinspun E, Hirani A, Desbrun M, Schröder P. Discrete shells. In: Proceedings of ACM SIGGRAPH/Eurographics symposium on computer animation. 2003. p. 62–7.
- [16] Etzmuss O, Gross J, Strasser W. Deriving a particle system from continuum mechanics for the animation of deformable objects. IEEE Transactions on Visualization and Computer Graphics 2003;9(4):538–50.
- [17] Eberhardt B, Etzmuss O, Hauth M. Implicit-explicit schemes for fast animation with particle systems. In: Proceedings of the Eurographics workshop on computer animation and simulation. 2000.
- [18] Kang Y-M, Choi J-H, Cho H-G, Park C-J. A fast and stable cloth animation with approximation of implicit method. In: Proceedings of computer graphics international. 2000. p. 247–55.
- [19] Hauth M, Etzmuss O. A high performance solver for the animation of deformable objects using advanced numerical methods. Computer Graphics Forum 2001;20(3):319–28.
- [20] Goldenthal R, Harmon D, Fattal R, Bercovier M, Grinspun E. Efficient simulation of inextensible cloth. ACM Transactions on Graphics (Proceedings of SIGGRAPH 2007) 2007;26(3).
- [21] Hormann K, Sheffer A, Levy B, Desbrun M, Zhou K. Mesh parameterization: Theory and practice. ACM SIGGRAPH 2007 Course Notes 2007.
- [22] Sheffer A, de Sturler E. Parameterization of faceted surfaces for meshing using angle based flattening. Engineering with Computers 2001;17(3):326–37.
- [23] Desbrun M, Meyer M, Alliez P. Intrinsic parameterizations of surface meshes. Computer Graphics Forum 2002;21(3):209–18.
- [24] Lee Y, Kim H-S, Lee S. Mesh parameterization with a virtual boundary. Computers & Graphics 2002;26(5):677–86.
- [25] Lévy B, Petitjean S, Ray N, Maillot J. Least squares conformal maps for automatic texture atlas generation. ACM Transactions on Graphics 2002;21(3):362–71.
- [26] Karni Z, Gotsman C, Gortler SJ. Free-boundary linear parameterization of 3D meshes in the presence of constraints. In: Proceedings of the international conference on shape modeling and applications 2005. 2005. p. 268–77.
- [27] Sheffer A, Lévy B, Mogilnitsky M, Bogomyakov A. ABF++: Fast and robust angle based flattening. ACM Transactions on Graphics 2005;24(2):311–30.
- [28] Zayer R, Lévy B, Seidel H-P. Linear angle based parameterization. In: Proceedings of ACM/Eurographics symposium on geometry processing. 2007.
- [29] Sander PV, Gortler SJ, Snyder J, Hoppe H. Signal-specialized parametrization. In: EGRW '02: Proceedings of the 13th Eurographics workshop on rendering. 2002. p. 87–98.
- [30] Tewari G, Snyder J, Sander PV, Gortler SJ, Hoppe H. Signal-specialized parameterization for piecewise linear reconstruction. In: SGP'04: Proceedings of the 2004 Eurographics/ACM SIGGRAPH symposium on geometry processing. 2004. p. 55–64.
- [31] Aono M, Breen D, Wozny M. Fitting a woven-cloth model to a curved surface: Mapping algorithms. Computer-Aided Design 1994;26:278–92.
- [32] Azariadis P, Aspragathos N. Design of plane development of doubly curved surface. Computer-Aided Design 1997;29:675–85.
- [33] McCartney J, Hinds B, Seow B. The flattening of triangulated surfaces incorporating darts and gussets. Computer-Aided Design 1999;31:249–60.
- [34] Aono M, Breen D, Wozny M. Modeling methods for the design of 3d broadcloth composite parts. Computer-Aided Design 2001;33:989–1007.
- [35] Wang CCL, Smith S, Yuen M. Surface flattening based on energy model. Computer-Aided Design 2002;34(11):823–33.
- [36] Wang CCL, Tang K, Yeung B. Freeform surface flattening by fitting a woven mesh model. Computer-Aided Design 2005;37:799–814.
- [37] Leopoldseder S, Pottmann H. Approximation of developable surfaces with cone spline surfaces. Computer-Aided Design 1998;30(7):571–82.
- [38] Pottmann H, Wallner J. Approximation algorithms for developable surfaces. Computer Aided Geometric Design 1999;16(9):539–56.
- [39] Chu C, Séquin C. Developable Bézier patches: Properties and design. Computer-Aided Design 2002;34(7):511–27.
- [40] Chen H, Lee I, Leopoldseder S, Pottmann H, Randrup T, Wallner J. On surface approximation using developable surfaces. Graphical Models and Image Processing 1999;61(2):110–24.
- [41] Peternell M. Recognition and reconstruction of developable surfaces from point clouds. In: Proceedings of geometric modeling and processing 2004. 2004. p. 301–10.
- [42] Peternell M, Steiner T. Reconstruction of piecewise planar objects from point clouds. Computer-Aided Design 2004;36(4):333–42.
- [43] Decaudin P, Julius D, Wither J, Boissieux L, Sheffer A, Cani M-P. Virtual garments: A fully geometric approach for clothing design. Computer Graphics Forum 2006;25(3):625–34.
- [44] Wang CCL, Tang K. Achieving developability of a polygonal surface by minimum deformation: A study of global and local optimization approaches. The Visual Computer 2004;20(8–9):521–39.
- [45] Wang CCL. Towards flattenable mesh surfaces. Computer-Aided Design 2008;40(1):109–22.
- [46] Liu Y, Pottmann H, Wallner J, Yang Y-L, Wang W. Geometric modeling with conical meshes and developable surfaces. ACM Transactions on Graphics 2006;25(3):681–9.
- [47] Wang CCL, Tang K. Woven model based geometric design of elastic medical braces. Computer-Aided Design 2007;29(1):69–79.
- [48] Dowling NE. Mechanical behavior of materials. New York: Prentice-Hall; 1993.
- [49] Fung YC. Foundations of solid mechanics. Englewood Cliffs (NJ): Prentice-Hall; 1965.
- [50] Madsen K, Nielsen H, Tingleff O. Optimization with constraints. Lecture notes, 2004.
- [51] Wang CCL. Computing length-preserved free boundary for quasi-developable mesh segmentation. IEEE Transactions on Visualization and Computer Graphics 2008;14(1):25–36.
- [52] Algor. 2008. <http://www.algor.com>.
- [53] Botsch M, Kobell L. A remeshing approach to multiresolution modeling. In: SGP'04: Proceedings of the 2004 Eurographics/ACM SIGGRAPH symposium on geometry processing. 2004. p. 185–92.